Quantitative Assessment of Articular Cartilage Morphology via EPIC-µCT

Liqin Xie, Ph.D.[+], **Angela S.P. Lin, M.S.**[+], **Marc E. Levenston, Ph.D.**[*], and **Robert E. Guldberg, Ph.D.**[+,1]

[+]*George W. Woodruff School of Mechanical Engineering, 315 Ferst Drive, Georgia Institute of Technology, Atlanta, GA 30332-0405*

[*]*Department of Mechanical Engineering, 233 Durand Building, Stanford University, Stanford, CA 94305-4038*

Summary

Objective—The objective of the present study was to validate the ability of EPIC-µCT to nondestructively assess cartilage morphology in the rat model.

Design—An appropriate contrast agent (Hexabrix) concentration and incubation time for equilibration were determined for reproducible segmentation of femoral articular cartilage from contrast-enhanced µCT scans. Reproducibility was evaluated by triplicate scans of six femora, and the measured articular cartilage thickness was independently compared to thickness determined from needle probe testing and histology. The validated technique was then applied to quantify age-related differences in articular cartilage morphology between 4, 8, and 16-week old (n=5 each) male Wistar rats.

Results—A 40% Hexabrix/60% PBS solution with 30 minute incubation was optimal for segmenting cartilage from the underlying bone tissue and other soft tissues in the rat model. High reproducibility was indicated by the low coefficient of variation (1.7-2.5%) in cartilage volume, thickness and surface area. EPIC-µCT evaluation of thickness showed a strong linear relationship and good agreement with both needle probing (r^2=0.95, slope=0.81, p<0.01, mean difference 11 ±22µm, n=43) and histology (r^2=0.99, slope=0.97, p<0.01, mean difference 12±10µm, n=30). Cartilage volume and thickness significantly decreased with age while surface area significantly increased.

Conclusion—EPIC-µCT imaging has the ability to nondestructively evaluate three-dimensional articular cartilage morphology with high precision and accuracy in a small animal model.

Keywords

EPIC-µCT; Cartilage morphology; Cartilage development; Cartilage imaging; Microcomputed tomography

---

Conflict of Interest Statement: The authors have no conflicts of interest to disclose.

Introduction

Osteoarthritis (OA) is the most common joint disorder and is characterized by a gradual but progressive loss of articular cartilage [1]. Interest in understanding disease pathogenesis in more detail and in developing efficient models for testing disease modifying therapies has motivated the development of small animal models for joint degeneration [2,3]. Accurately quantifying morphologic changes in small animals is a critical factor in the development and evaluation of new therapies for osteoarthritis. However, existing technologies for assessing articular cartilage morphology are typically destructive and time-consuming or limited by inadequate spatial resolution.

Morphologic changes in articular joint cartilage can be destructively evaluated via histology, needle probing [4,5], and stereophotographic techniques [6], but these methods do not allow repetitive analysis in the same sample. Nondestructive articular cartilage assessment techniques, including magnetic resonance imaging (MRI) [7,8], and ultrasonography [4], are capable of monitoring cartilage changes in humans, but do not usually provide adequate resolution for the thinner articular cartilage in small animal joints. Optical coherence tomography (OCT) is capable of imaging rat cartilage at high resolution [9-11], but only provides two-dimensional images. A nondestructive, high resolution technique that provides accurate and precise (i.e. reproducible) quantification of cartilage morphologic parameters such as volume, surface area, and thickness would be tremendously valuable for small animal studies of joint degeneration [12,13].

Microcomputed tomography (μCT) provides three-dimensional (3-D), quantitative morphologic analysis of hard tissues at micron-level voxel resolutions and has become the "gold standard" for bone microstructural analysis. However, soft tissues such as cartilage are generally undetectable by μCT due to their low X-ray attenuation, and segmentation of cartilage from other soft tissues in such images is not possible. μCT arthrography has been used previously for *ex vivo* visualization of the rat patellar cartilage thickness [14]. Recently, Equilibrium Partitioning of an Ionic Contrast agent via μCT (EPIC-μCT), a nondestructive imaging technique combining μCT with a charged X-ray-absorbing contrast agent, has been shown to provide direct *in situ* visualization of articular cartilage morphology in a rabbit femur [15]. The objective of the present study was to evaluate the ability of EPIC-μCT to nondestructively assess cartilage thickness and morphology in the much thinner cartilage of the rat. Specifically, this study addressed the following research issues: (1) the appropriate incubation conditions for the contrast agent (Hexabrix) to optimize identification of cartilage in μCT images, (2) a suitable segmentation method to reliably distinguish cartilage from bone and non-cartilage soft tissues, and (3) the precision (reproducibility) of this novel technique to assess cartilage morphology and agreement with two independent thickness measurements. Finally, EPIC-μCT was applied to quantify age-related morphologic differences in rat articular cartilage during postnatal growth from 4 to 16 weeks of age.

Methods

Contrast agent concentration and incubation time

Twelve femora were harvested from six 8-week old male Wistar rats (Charles River Laboratories, Sparks, NV) and kept in phosphate buffered saline (PBS) at 4°C. To prevent cartilage degeneration, the PBS used throughout this study contained protease inhibitors (1% Protease Inhibitor Cocktail Set I, CalBiochem, San Diego, CA). After dissection of surrounding tissue, each femur was pre-scanned prior to incubation with the contrast medium. The distal femur was then immersed in 2 ml of a specified dilution in PBS of the ionic CT contrast agent Hexabrix 320 (Mallinckrodt, Hazelwood, MO) for 5 minutes at 37°C, then patted dry and immediately transferred to the μCT system for scanning. The femur was then removed,

immersed in the contrast agent solution for another 5 minutes, and then rescanned. For each sample, this process was repeated for cumulative immersion times of 0, 5, 10, 15, 30, and 60 minutes to identify the time required to reach equilibrium. This procedure was repeated for femora (n=3) incubated in one of four contrast agent dilutions: 20% Hexabrix/80% PBS, 30% Hexabrix/70% PBS, 40% Hexabrix/60% PBS or 50% Hexabrix/50% PBS.

All femora were consistently secured such that the longitudinal axis was aligned with the vertical axis of the μCT scanning tube. The scanning tube, containing PBS at the bottom, was sealed with parafilm to prevent dehydration during scanning. All scanning was performed in air using a μCT 40 (Scanco Medical, Bassersdorf, Switzerland) at 45 kVp, 177 μA, 200ms integration time, and a voxel size of 12 μm with a 12 mm scanning tube. Approximately 360 slices (4.3mm) of each distal femur were scanned. For the convenience of histogram analysis, a volume of interest (VOI) was defined for each condyle extending from the top surface of the cartilage down 31 slices, or 372 μm, which included cartilage, subchondral bone, and some trabecular bone. By using Scanco Medical software, a histogram of the X-ray attenuation values was produced, revealing two partially overlapping peaks corresponding to contrast-enhanced articular cartilage and calcified bone. Separation of the midpoint attenuation values from bone and cartilage peaks in the histograms were directly compared at equilibrium for the four contrast agent concentrations. Cartilage attenuation for each femur was determined by averaging values from both condyles.

Scanning and segmentation procedures

Based on results of the parametric studies (see below), incubation for 30 minutes in 40% Hexabrix/60% PBS at 37°C was selected as a standard incubation protocol. Subsequent analyses indicated that this protocol was also adequate to reach equilibrium in femoral articular cartilage from 4-week and 16-week old rats. A 16mm scanning tube was required to fit the largest samples in the study from 16-week old animals. All femora in the remaining studies were therefore evaluated in a 16 mm scanning tube, providing a voxel size of 16 μm, and scanned at 45 kVp, 177 μA, 200 ms integration time, and 25-40 minute acquisition time.

The femora were placed in a vertical position during scanning, and the μCT scanner therefore produced transverse cross-sectional slices. Cartilage, subchondral bone, and bone marrow were adjacent in the regions of analysis. Because Hexabrix diffuses into marrow, giving it similar attenuation values to cartilage, a global threshold for segmentation in the whole distal femur was not suitable. In order to accurately segment the femoral articular cartilage from bone marrow, contour lines for articular cartilage were manually drawn. Semi-automatic contouring was applied every 3-10 slices. However, semi-automatic contouring was not feasible for all the cross-sectional slices due to the curved morphology of articular cartilage and disconnected sections in these images (Fig. 1A). In addition, a pilot study showed that partial volume effects in the cross-sectional images produced inaccurate cartilage boundaries in the central regions of both femoral condyles. To overcome this challenge, a new segmentation method was developed. By using Scanco Medical software, the femoral bulk image (grayscale image file) was 3-D rotated to ensure that the lateral-medial axis was aligned with the vertical axis. The femoral bulk image was re-sliced horizontally via manual reconstruction, to generate a series of sagittal sections (Fig. 1B). After drawing contour lines to eliminate marrow space (Fig. 1C), an appropriate threshold was selected to segment cartilage from bone tissue according to the histogram analysis of the tissues (Fig. 1D). The lower threshold was 70, and the upper threshold was 220 (Gauss filter parameters: sigma=1.2, support=2). The 3-D morphology of the entire articular cartilage layer was then visualized (Fig. 1E) and quantified in terms of average cartilage thickness, volume, and surface area using direct distance transformation algorithms [16,17]. In addition, a thickness map of the soft tissue volume was generated and presented as a pseudo color-scaled image.

Precision evaluation

To evaluate the reproducibility of measuring cartilage morphology via EPIC-μCT, four femora from 4-week old rats and two femora from 8-week old rats were scanned three times in two days. The distal femora were incubated in 40% Hexabrix/60% PBS for 30 minutes at 37°C and scanned as described above. After desorption of the contrast agent for 1 hour in PBS, the femora were re-incubated with contrast agent and re-scanned. The specimens were stored in PBS at 4°C overnight until the third scan, which was performed on the second day. The cartilage volume, thickness and surface area of the three measurements were compared, and the coefficient of variation (100 times the standard deviation divided by the mean of the three measurements) was calculated for each sample. The root mean square coefficient of variation (RMS-CV) and root mean square standard deviation (RMS-SD) [18] were averaged for the 6 samples. All scans and analyses were performed by a single experienced operator.

Thickness validation via needle probing

Cartilage thicknesses for five specimens (2 femora, 3 tibiae) from three additional rats were measured by slow (0.006 mm/s) insertion of a blunt needle probe (~0.1mm in diameter) attached to a 5 N load cell (sensitivity: 0.001N, Interface, Scottsdale, AZ) on an ELF3100 mechanical test frame (EnduraTec, Minnetonka, MN). The load and displacement outputs were recorded at 3 Hz as the needle penetrated into the cartilage tissue. A change from zero to non-zero slope on the load-displacement chart indicated contact with the cartilage surface and a sudden rise in force indicated contact with bone. The articular surface was kept hydrated with PBS solution. After probing, each sample was examined via EPIC-μCT and the thickness at each probe location (based on manual marking) was measured in the 3-D viewing window of the Scanco Medical software interface.

Morphology of 4, 8, and 16-week old rat femora and histology comparison

Three groups of male Wistar rats of different ages (4, 8, and 16-week old, n=5 each) were sacrificed and both femora were harvested. The distal femora were incubated and scanned according to the standard protocol described above. Following μCT scanning, femora were fixed fresh in 10% neutral buffered formalin overnight and decalcified in 2.5% formic acid (pH 4.2) for 10 days. Upon dehydration, samples were embedded in glycol methacrylate (GMA) according to the manual of the JB-4 embedding kit (Polysciences, Warrington, PA). For comparison with the 3-D spatial images generated by EPIC-μCT, sagittal sections were cut at 8μm thickness, and the central sections of each condyle were examined. Sections were stained for sulfated glycosaminoglycans (sGAGs) by using a 0.5% safranin-O solution with a 0.2% aqueous solution of fast green used as a counterstain. For each femur, one central, sagittal section in each condyle was used for the thickness analysis. Digital images of each section were captured at a resolution of 0.5μm. The cartilage thickness of each section was defined as the average value of 10 manual thickness measurements at regular intervals perpendicular to the cartilage surface (Image J, NIH). Femoral articular cartilage thickness was determined by averaging values from both condyles.

Statistical analysis

All data were expressed as mean ± standard deviation. Average cartilage morphology parameters during growth were evaluated using a one factor (age) repeated (left vs. right) general linear model with Tukey's test for post-hoc analysis. The histology measurements of cartilage thickness during growth were evaluated via one-way ANOVA with Tukey's test for post-hoc analysis. Thickness measurements via EPIC-μCT and needle probing/histology were compared via paired t-tests, and the relationships and agreements between these two methods were examined via linear regression analysis and Bland-Altman analysis [19], separately. Statistical significance was set at $p = 0.05$ (SPSS 11, SPSS Inc., Chicago, IL).

Results

Appropriate incubation time and Hexabrix concentration were determined from analysis of average attenuation for femoral articular cartilage after incubation with four concentrations of Hexabrix solution. The average attenuation of femoral articular cartilage without incubation (65, expressed in threshold units) was close to that of PBS (58). Attenuation within the cartilage increased quickly during incubation at each concentration of Hexabrix solution, and reached a plateau in less than 30 min (Fig. 2B). Attenuation histograms (Fig. 2C-F) showed that lower Hexabrix concentrations increased the separation between peaks of cartilage and bone. After equilibration, the average attenuation (216) of the cartilage incubated with 50% Hexabrix was too similar to that of bone (265) to allow reproducible segmentation (Fig. 2B,C). The average attenuation of the cartilage incubated with 40% Hexabrix was 199 (Fig. 2B), and the histogram analysis (Fig. 2D) demonstrated that it was feasible to segment bone and cartilage using 40% Hexabrix. The average attenuations of the cartilage incubated with 30% or 20% Hexabrix were 168 and 128 respectively (Fig. 2E,F), which also allowed segmentation between bone and cartilage but provided less contrast difference for accurately detecting the cartilage surface. Though the goals of this study did not include using the Hexabrix contrast procedure for assessing sGAG distribution within the cartilage, this application is of interest. Higher Hexabrix concentrations allow for increased sensitivity to changes in sGAG content [15], therefore the highest concentration of Hexabrix that allowed segmentation between cartilage and bone was chosen as optimal.

The root mean square coefficient of variation (RMS-CV) determined by triplicate scanning of six samples was 2.5%, 1.5%, and 1.7% for cartilage volume, thickness, and surface area, respectively. The root mean square standard deviation (RMS-SD) was 0.46 mm^3 for cartilage volume, 7.3 μm for the thickness, and 1.39 mm^2 for surface area.

Cartilage thickness determined via needle probe testing was not significantly different from measurements provided via EPIC-μCT (paired t-test, p=0.25) (Fig. 3). The average thickness of the articular cartilage from the 43 probing points was 202±79 μm and 191±66 μm for the needle probe and EPIC-μCT techniques, respectively. Linear regression analysis of thickness measurements from EPIC-μCT and needle probing revealed a strong linear relationship (r^2=0.95, slope=0.81, p<0.01, n=43). Bland-Altman analysis demonstrated good agreement between these two methods for thickness measurements, with an average thickness difference of 11±22μm and 95% limits of agreement -30 to 50μm.

Representative images of 3-D morphology of rat articular cartilage as a function of age are shown in Fig. 4, including 3-D thickness distribution maps. The mean of relative differences (absolute difference between left and right femora divided by the mean of both femora) for the three morphologic parameters was calculated [12]. The values ranged from 1.6% to 4.4% in each age group, and no differences between right and left limbs were significant. From 4 to 8 weeks of age, cartilage volume and thickness decreased by 37.9% and 57.5% (both p<0.01), respectively, while cartilage surface area increased by 35.6% (p<0.01). Normal growth from 8 to 16 weeks further decreased articular cartilage volume and cartilage thickness by 26.6% and 35.0% (both p<0.01), respectively, and further increased cartilage surface area by 17.6% (p<0.01).

Representative images of femoral articular cartilage sections stained with safranin-O are shown in Fig. 5. Thickness measurements from EPIC-μCT indicated that the average thickness of the left and right femur decreased from 403±11μm to 171±15μm during normal growth from 4 to 8 weeks, and further decreased to 111±8μm at 16 weeks. Similarly, thickness measurement via histology images indicated that the thickness decreased from 420±19μm to 180±14μm during normal growth from 4 to 8 weeks, and further decreased to 122±13μm at 16 weeks.

Thickness measurements from EPIC-μCT and histology images showed good correlation for each age group (4-week: r^2=0.64, 8-week: r^2=0.66, 16-week: r^2=0.70; p<0.01, n=10), with a strong linear relationship across all three age groups (r^2=0.99, slope=0.97, p<0.01, n=30). Bland-Altman analysis demonstrated good agreement between these two methods for thickness measurements, with an average thickness difference of 12±10μm and 95% limits of agreement -8 to 32μm across all three age groups.

Discussion

Experimental small animal models are necessary and complementary to large animal and clinical studies. Small animal models of arthritis are well suited for understanding pathogenesis and therefore benefit the development of disease modifying drugs. However, current analysis methods may not provide adequate sensitivity for detecting morphologic changes in the cartilage of small animals. To expand the ability of EPIC-μCT to assess cartilage morphology in small animals, this study determined incubation and scanning conditions and developed an effective segmentation method. The results confirmed the high precision and accuracy of this technique, and illustrated that EPIC-μCT imaging provides the ability to nondestructively assess morphologic changes in rat articular cartilage associated with growth and maturation from 4 to 16 weeks.

This study determined an optimal incubation period and contrast agent concentration for assessing the morphology of rat femoral articular cartilage. The equilibration time is a function of the effective diffusivity of the contrast agent and the thickness of the tissue. The results of the incubation condition experiment suggested that 30 minutes of incubation was sufficient for the contrast solution to equilibrate in rat femoral articular cartilage, regardless of concentration. However, it must be noted that specimens of other species and sizes would require separate optimization. The contrast between tissues is based on their relative X-ray attenuation [20]. The optimal Hexabrix concentration was identified as the concentration that produced sufficient attenuation differences between cartilage and bone while still providing enough contrast above background to allow consistent definition of the articular surface. Incubation with 50% Hexabrix increased the radiopacity of cartilage to a level that was too similar to that of bone, and reproducible identification of the tissue interface was not possible. Concentrations of 20-40% Hexabrix allowed successful segmentation between bone and cartilage in the rat joint. Although the goal of the present study was not to assess the composition of the cartilage, selecting a contrast agent concentration that allowed both segmentation and high sensitivity to variations in sGAG content was desirable. Higher concentrations provided greater sensitivity for sGAG content measurements [15]. 40% Hexabrix was the highest concentration that allowed segmentation of bone and cartilage as well as high sensitivity to sGAG concentration and cartilage surface definition. Therefore, 40% Hexabrix and a 30 minutes incubation time were chosen as the optimal incubation conditions for rat femoral articular cartilage.

Accuracy and precision are essential for quantifying cartilage morphology in joint degeneration and for testing disease modifying therapies [18,21,22]. Several factors could influence the overall precision and reproducibility of EPIC-μCT analyses. These include potential inconsistencies in sample preparation (Hexabrix incubation, scan position, Hexabrix desorption from cartilage, cartilage tissue degeneration, change in cartilage water content) as well as image analysis (3-D image rotations, partial volume effects, and manual drawing of contour lines). Although the absolute correct value for cartilage thickness is not known, good agreement was found between EPIC-μCT measurements of cartilage thickness and two independent destructive techniques. Strong linear relationships existed between EPIC-μCT thickness measures and those provided by needle probe testing and histology. The small coefficients of variation (CV, 1.7-2.5%) and standard deviations demonstrated the high level of precision for the EPIC-μCT technique. The variability in this study was much less than that

from studies employing clinical MRI (CV up to 7.9%) [23] or micro-MRI (CV up to 8.3%) [21]. Given the high reproducibility in our study, a power analysis showed that the EPIC-µCT technique is expected to have 80% power and 95% confidence to detect a 1.3% thickness change with a sample size of 10. The high precision was further indirectly validated by the small mean relative difference (<5%) in cartilage morphology between left and right femora. These differences account for the error variance between the two scans and evaluations as well as biological differences between limbs of a single animal [24].

Though 2-D histomorphometry is still the accepted standard for measuring cartilage thickness, 3-D morphometric analyses obtained through EPIC-µCT offer several distinct advantages: eliminating the need for exact specimen positioning and alignment [25], providing more precise thickness measurements via sphere fitting in the tissue space perpendicular to the curved cartilage surface [6,16], and providing a more complete volumetric assessment throughout the entire cartilage layer. In addition, histologic processing, fixation, dehydration, and embedding may produce artifacts in cartilage thickness measurements [26]. EPIC-µCT is nondestructive, and the contrast agent (Hexabrix) is easily desorbed. Therefore, most standard histologic processes can still be performed upon completion of EPIC-µCT scanning. However, there are a few notable limitations of the EPIC-µCT technique. One limitation is the time required to manually draw contours on hundreds of slices (30-60 minutes for one femoral sample). An automated, computer-based segmentation method would be more efficient and could potentially provide higher reproducibility due to the elimination of inter/intra-reader variation [12,27]. Feasibility was only verified on fresh cartilage samples. The integrity of fresh cartilage samples can only be retained for several days with protease inhibitors. While it should be possible to analyze fixed or frozen samples, this was not examined in the current study.

MRI techniques have been clinically used to successfully quantify articular cartilage morphology, volume, and thickness and to identify focal defects [18,28]. Recently micro-MRI has been used to evaluate patellar cartilage morphologic changes in small animals [7,8], but the resolution ($31 \times 31 \times 100 \mu m^3$) is too low for the curved femoral articular cartilage in rats. In addition, the cost and availability of micro-MRI instruments are significant limitations. µCT scanners are more readily available, and the resolution [29] is significantly better than that of MRI [7,8]. No significant morphologic distortions have been reported in CT [30] while such artifacts have been apparent in MR images [20,31]. The appropriate contrast agent concentration enables reproducible segmentation of articular cartilage from bone in EPIC-µCT scans.

EPIC-µCT was utilized to detect a decrease in average cartilage thickness in rat distal femora during postnatal growth. This decrease in thickness during growth, which can be attributed to endochondral bone development, is consistent with previous histologic, ultrasonic, and needle probe studies [32,33]. EPIC-µCT analysis also showed that the femoral articular cartilage volume decreased during growth while the cartilage surface area increased. These data illustrate the capability of EPIC-µCT to assess morphologic changes in rat articular cartilage. Although this study only compared the average morphometric parameters of the entire femoral articular cartilage layer, it is also feasible to quantify local morphologic variations by selecting regional volumes of interest. In addition, the technique can easily be extended to analyze other cartilaginous regions or other soft tissues containing substantial levels of sGAGs.

Failure to completely assess articular cartilage morphology through existing techniques has limited the development of new treatments for osteoarthritis [12]. Although this validation study focused on cartilage development, the potential significance of our work to the field of osteoarthritis research is apparent, including understanding the progression of cartilage degeneration and evaluating the effect of potential osteoarthritis drugs. For osteoarthritis, the reproducibility of thickness and volume measurements via EPIC-µCT may decrease because

of the low average thicknesses and volumes caused by disease [18,34]. The attenuation of cartilage will increase because of the loss of sGAG content [15,35], and the segmentation of cartilage from bone may be more difficult because of the overlap of attenuation peaks for these two tissues. However, high attenuation within a focal defect could make it more detectable compared to adjacent normal cartilage with lower attenuation. A recent study indicated that contrast enhanced in vivo μCT was able to detect decreases in cartilage volume and sGAG content in rat patellae in an experimental osteoarthritis model [35]. EPIC-μCT may therefore represent a powerful new tool for analyzing the progression and treatment of arthritis in small animal models.

This was the first study to present 3-D thickness and topography mappings for femoral articular cartilage in a rodent model. Using high resolution 3-D cartilage thickness maps, focal variations in cartilage thickness can be visualized via the color scale, and the cartilage contact area and surface stresses can be estimated [6,21]. The thickness and topography maps can also be used to evaluate joint mechanics and mechano-adaptation of articular cartilage [36]. In addition, these maps could be utilized to define the relationship between genetic background and cartilage phenotype [37], and also provide guidance in the design of prosthetic surfaces and tissue engineering constructs.

In summary, this study established the basis for a quantitative, high resolution, 3-D imaging technique capable of nondestructively assessing cartilage morphology with high precision. EPIC-μCT imaging has the potential to be applied broadly, similar to the application of μCT in bone structural analysis, and become a gold standard for articular cartilage morphology assessment in small animal models.

Acknowledgements

References

1. Goldring SR, Goldring MB. Clinical aspects, pathology and pathophysiology of osteoarthritis. J Musculoskelet Neuronal Interact 2006;6:376–378. [PubMed: 17185832]

2. Bendele AM. Animal models of osteoarthritis. J Musculoskelet Neuronal Interact 2001;1:363–376. [PubMed: 15758487]

3. Wooley PH. The usefulness and the limitations of animal models in identifying targets for therapy in arthritis. Best Pract Res Clin Rheumatol 2004;18:47–58. [PubMed: 15123037]

4. Jurvelin JS, Rasanen T, Kolmonen P, Lyyra T. Comparison of optical, needle probe and ultrasonic techniques for the measurement of articular cartilage thickness. J Biomech 1995;28:231–235. [PubMed: 7896866]

5. Roemhildt ML, Coughlin KM, Peura GD, Fleming BC, Beynnon BD. Material properties of articular cartilage in the rabbit tibial plateau. J Biomech 2006;39:2331–2337. [PubMed: 16168420]

6. Millington SA, Grabner M, Wozelka R, Anderson DD, Hurwitz SR, Crandall JR. Quantification of ankle articular cartilage topography and thickness using a high resolution stereophotography system. Osteoarthritis Cartilage 2007;15:205–211. [PubMed: 16949841]

7. Watrin A, Ruaud JP, Olivier PT, Guingamp NC, Gonord PD, Netter PA, et al. T2 mapping of rat patellar cartilage. Radiology 2001;219:395–402. [PubMed: 11323463]

8. Watrin-Pinzano A, Ruaud JP, Olivier P, Grossin L, Gonord P, Blum A, et al. Effect of proteoglycan depletion on T2 mapping in rat patellar cartilage. Radiology 2005;234:162–170. [PubMed: 15564387]

9. Patel NA, Zoeller J, Stamper DL, Fujimoto JG, Brezinski ME. Monitoring osteoarthritis in the rat model using optical coherence tomography. IEEE Trans Med Imaging 2005;24:155–159. [PubMed: 15707241]

10. Roberts MJ, Adams SB Jr, Patel NA, Stamper DL, Westmore MS, Martin SD, et al. A new approach for assessing early osteoarthritis in the rat. Anal Bioanal Chem 2003;377:1003–1006. [PubMed: 14564447]

11. Yang Y, Whiteman S, Gey van Pittius D, He Y, Wang RK, Spiteri MA. Use of optical coherence tomography in delineating airways microstructure: comparison of OCT images to histopathological sections. Phys Med Biol 2004;49:1247–1255. [PubMed: 15128202]

12. Dam EB, Folkesson J, Pettersen PC, Christiansen C. Automatic morphometric cartilage quantification in the medial tibial plateau from MRI for osteoarthritis grading. Osteoarthritis Cartilage 2007;15:808–818. [PubMed: 17353132]

13. Folkesson J, Dam EB, Olsen OF, Christiansen C. Accuracy evaluation of automatic quantification of the articular cartilage surface curvature from MRI. Acad Radiol 2007;14:1221–1228. [PubMed: 17889339]

14. Roemer FW, Mohr A, Lynch JA, Meta MD, Guermazi A, Genant HK. Micro-CT arthrography: a pilot study for the ex vivo visualization of the rat knee joint. AJR Am J Roentgenol 2005;184:1215–1219. [PubMed: 15788597]

15. Palmer AW, Guldberg RE, Levenston ME. Analysis of cartilage matrix fixed charge density and three-dimensional morphology via contrast-enhanced microcomputed tomography. Proc Natl Acad Sci U S A 2006;103:19255–19260. [PubMed: 17158799]

16. Laib A, Barou O, Vico L, Lafage-Proust MH, Alexandre C, Rugsegger P. 3D microcomputed tomography of trabecular and cortical bone architecture with application to a rat model of immobilisation osteoporosis. Med Biol Eng Comput 2000;38:326–332. [PubMed: 10912350]

17. Hildebrand T, Ruegsegger P. Quantification of Bone Microarchitecture with the Structure Model Index. Comput Methods Biomech Biomed Engin 1997;1:15–23. [PubMed: 11264794]

18. Eckstein F, Cicuttini F, Raynauld JP, Waterton JC, Peterfy C. Magnetic resonance imaging (MRI) of articular cartilage in knee osteoarthritis (OA): morphological assessment. Osteoarthritis Cartilage 2006;14:A46–75. [PubMed: 16713720]

19. Bland JM, Altman DG. Measuring agreement in method comparison studies. Stat Methods Med Res 1999;8:135–160. [PubMed: 10501650]

20. Haubner M, Eckstein F, Schnier M, Losch A, Sittek H, Becker C, et al. A non-invasive technique for 3-dimensional assessment of articular cartilage thickness based on MRI. Part 2: Validation using CT arthrography. Magn Reson Imaging 1997;15:805–813. [PubMed: 9309611]

21. Koo S, Gold GE, Andriacchi TP. Considerations in measuring cartilage thickness using MRI: factors influencing reproducibility and accuracy. Osteoarthritis Cartilage 2005;13:782–789. [PubMed: 15961328]

22. Gandy SJ, Dieppe PA, Keen MC, Maciewicz RA, Watt I, Waterton JC. No loss of cartilage volume over three years in patients with knee osteoarthritis as assessed by magnetic resonance imaging. Osteoarthritis Cartilage 2002;10:929–937. [PubMed: 12464553]

23. Hardya PA, Newmark R, Liu YM, Meier D, Norris S, Piraino DW, et al. The influence of the resolution and contrast on measuring the articular cartilage volume in magnetic resonance images. Magn Reson Imaging 2000;18:965–972. [PubMed: 11121699]

24. Muhlbauer R, Lukasz TS, Faber TS, Stammberger T, Eckstein F. Comparison of knee joint cartilage thickness in triathletes and physically inactive volunteers based on magnetic resonance imaging and three-dimensional analysis. Am J Sports Med 2000;28:541–546. [PubMed: 10921647]

25. Xia Y. The total volume and the complete thickness of articular cartilage determined by MRI. Osteoarthritis Cartilage 2003;11:473–474. [PubMed: 12814609]

26. Uchiyama T, Tanizawa T, Muramatsu H, Endo N, Takahashi HE, Hara T. A morphometric comparison of trabecular structure of human ilium between microcomputed tomography and conventional histomorphometry. Calcif Tissue Int 1997;61:493–498. [PubMed: 9383277]

27. Lublinsky S, Ozcivici E, Judex S. An automated algorithm to detect the trabecular-cortical bone interface in micro-computed tomographic images. Calcif Tissue Int 2007;81:285–293. [PubMed: 17828460]

28. Eckstein F. Noninvasive study of human cartilage structure by MRI. Methods Mol Med 2004;101:191–217. [PubMed: 15299216]

29. Schneider P, Stauber M, Voide R, Stampanoni M, Donahue LR, Muller R. Ultrastructural properties in cortical bone vary greatly in two inbred strains of mice as assessed by synchrotron light based micro- and nano-CT. J Bone Miner Res 2007;22:1557–1570. [PubMed: 17605631]

30. Sumanaweera T, Glover G, Song S, Adler J, Napel S. Quantifying MRI geometric distortion in tissue. Magn Reson Med 1994;31:40–47. [PubMed: 8121267]

31. Glaser C, Tins BJ, Trumm CG, Richardson JB, Reiser MF, McCall IW. Quantitative 3D MR evaluation of autologous chondrocyte implantation in the knee: feasibility and initial results. Osteoarthritis Cartilage 2007;15:798–807. [PubMed: 17363296]

32. Brommer H, Brama PA, Laasanen MS, Helminen HJ, van Weeren PR, Jurvelin JS. Functional adaptation of articular cartilage from birth to maturity under the influence of loading: a biomechanical analysis. Equine Vet J 2005;37:148–154. [PubMed: 15779628]

33. Meachim G, Bentley G, Baker R. Effect of age on thickness of adult patellar articular cartilage. Ann Rheum Dis 1977;36:563–568. [PubMed: 596949]

34. Burgkart R, Glaser C, Hyhlik-Durr A, Englmeier KH, Reiser M, Eckstein F. Magnetic resonance imaging-based assessment of cartilage loss in severe osteoarthritis: accuracy, precision, and diagnostic value. Arthritis Rheum 2001;44:2072–2077. [PubMed: 11592369]

35. Piscaer TM, Waarsing JH, Kops N, Pavljasevic P, Verhaar JA, van Osch GJ, et al. In vivo imaging of cartilage degeneration using muCT-arthrography. Osteoarthritis Cartilage. 2008

36. Eckstein F, Reiser M, Englmeier KH, Putz R. In vivo morphometry and functional analysis of human articular cartilage with quantitative magnetic resonance imaging--from image to data, from data to theory. Anat Embryol (Berl) 2001;203:147–173. [PubMed: 11303902]

37. Botter SM, van Osch GJ, Waarsing JH, van der Linden JC, Verhaar JA, Pols HA, et al. Cartilage damage pattern in relation to subchondral plate thickness in a collagenase-induced model of osteoarthritis. Osteoarthritis Cartilage. 2007
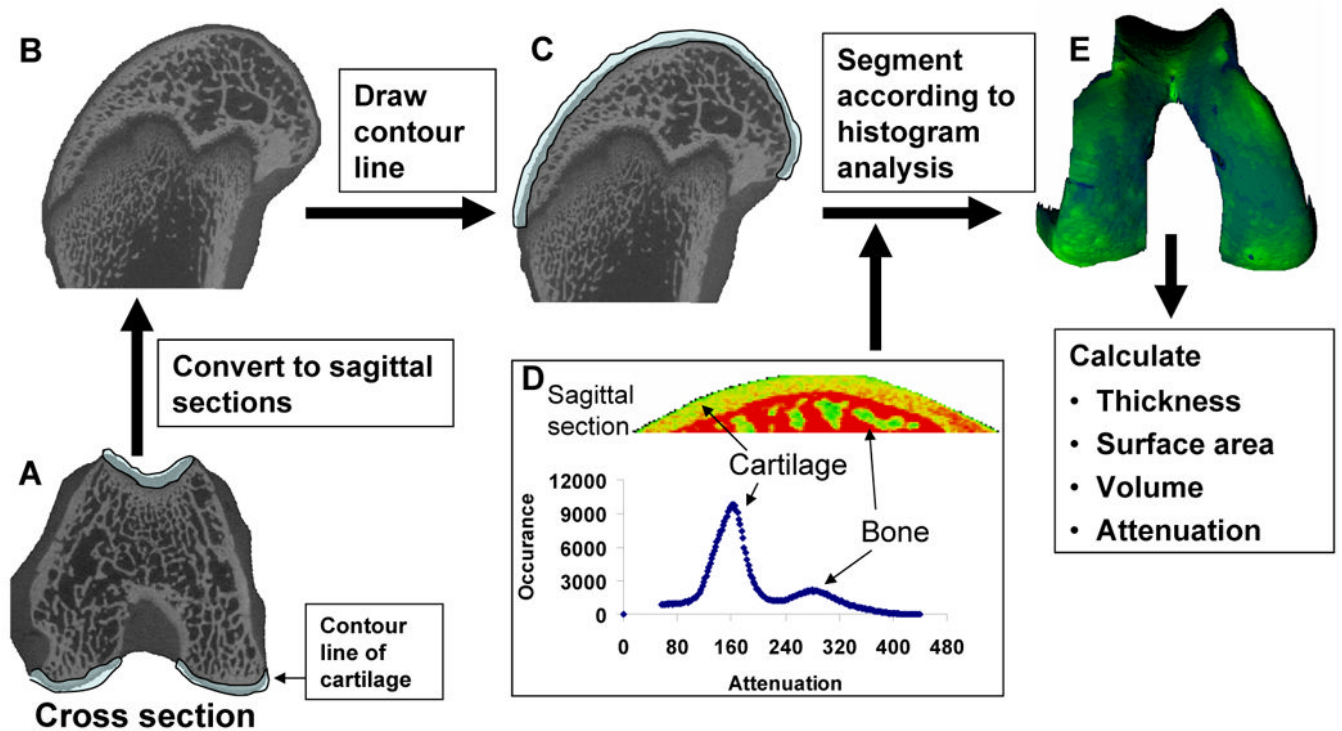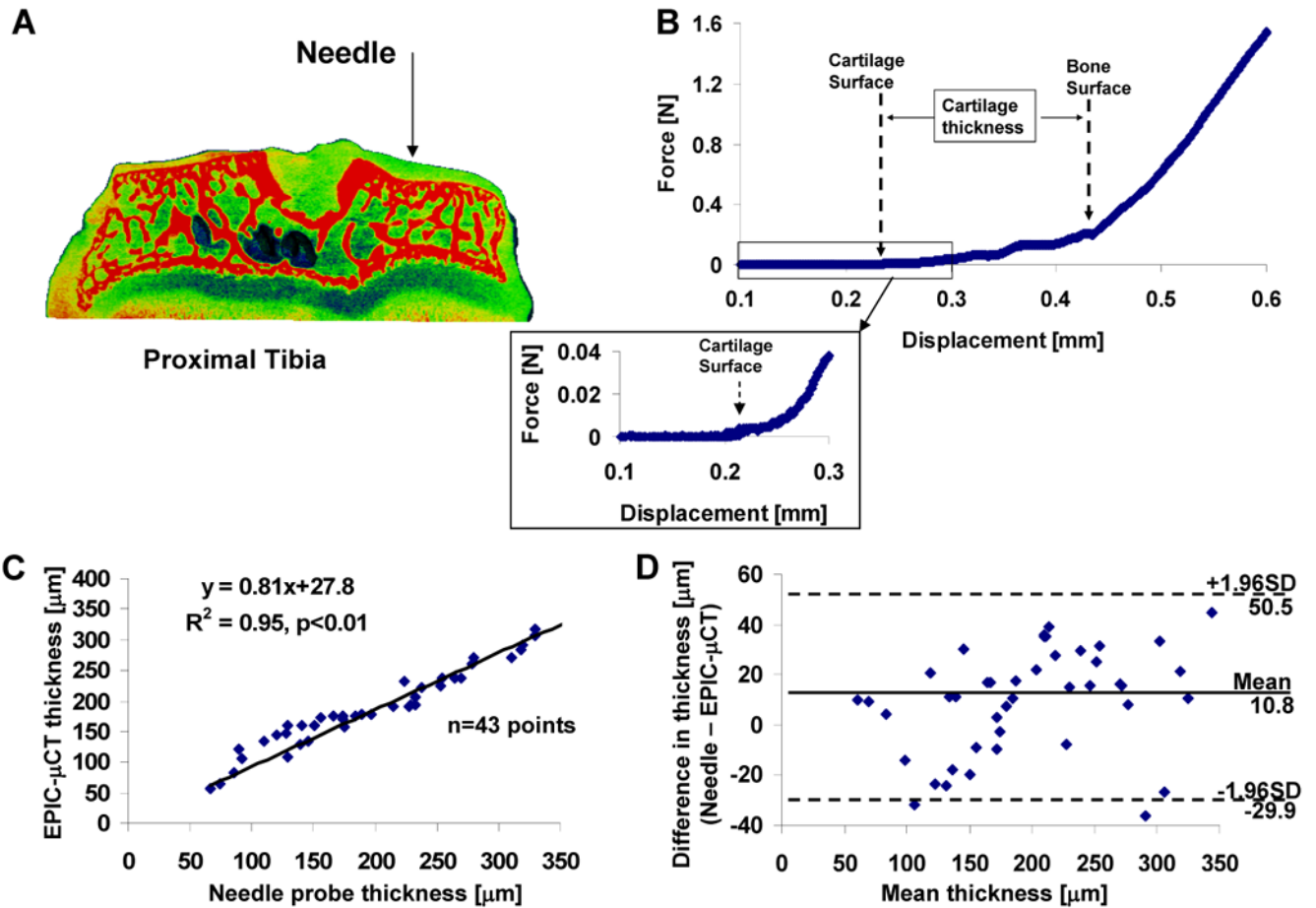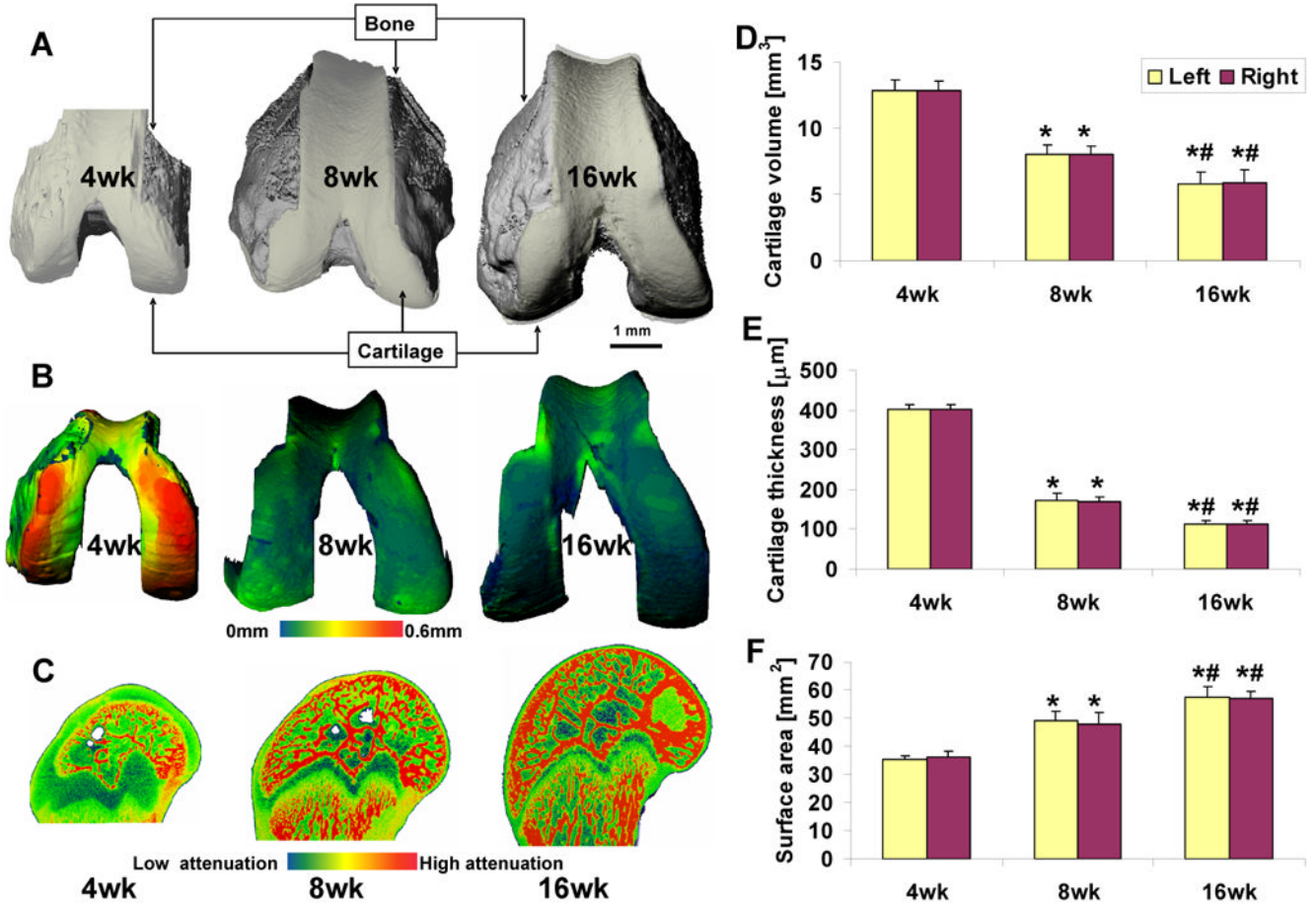
Figure 1.
The segmentation method for quantifying articular cartilage morphology in the rat distal femur. Femoral cross sections (A) were transformed into sagittal sections (B) via 3-D rotation of the grayscale image file. After drawing the contour lines to eliminate any adjacent bone marrow space (C), an appropriate threshold range was selected to segment cartilage from bone tissue according to the histogram analysis of the tissues (D). The 3-D morphology of articular cartilage was then visualized (E) and quantified in terms of cartilage thickness, volume, and surface area.
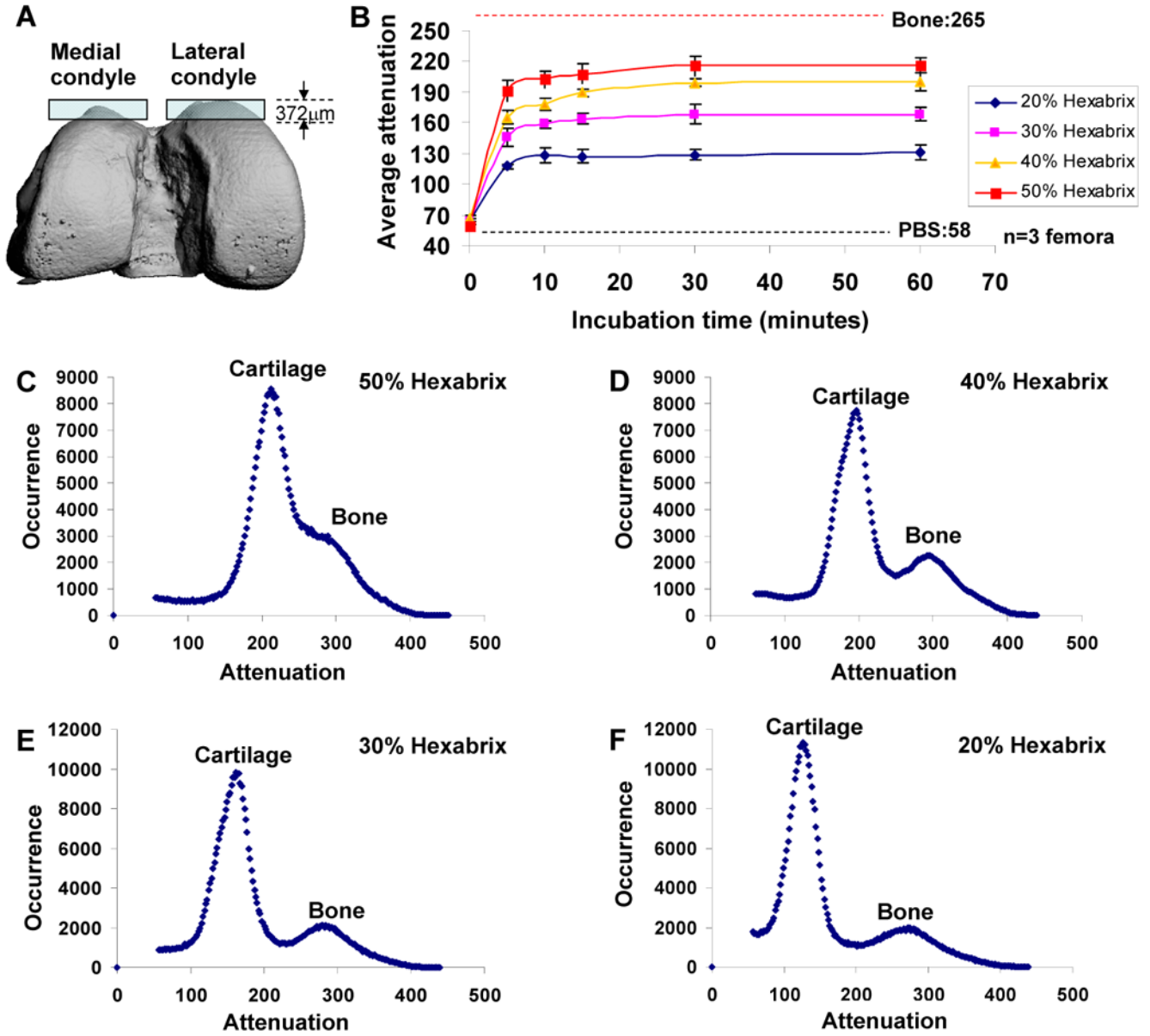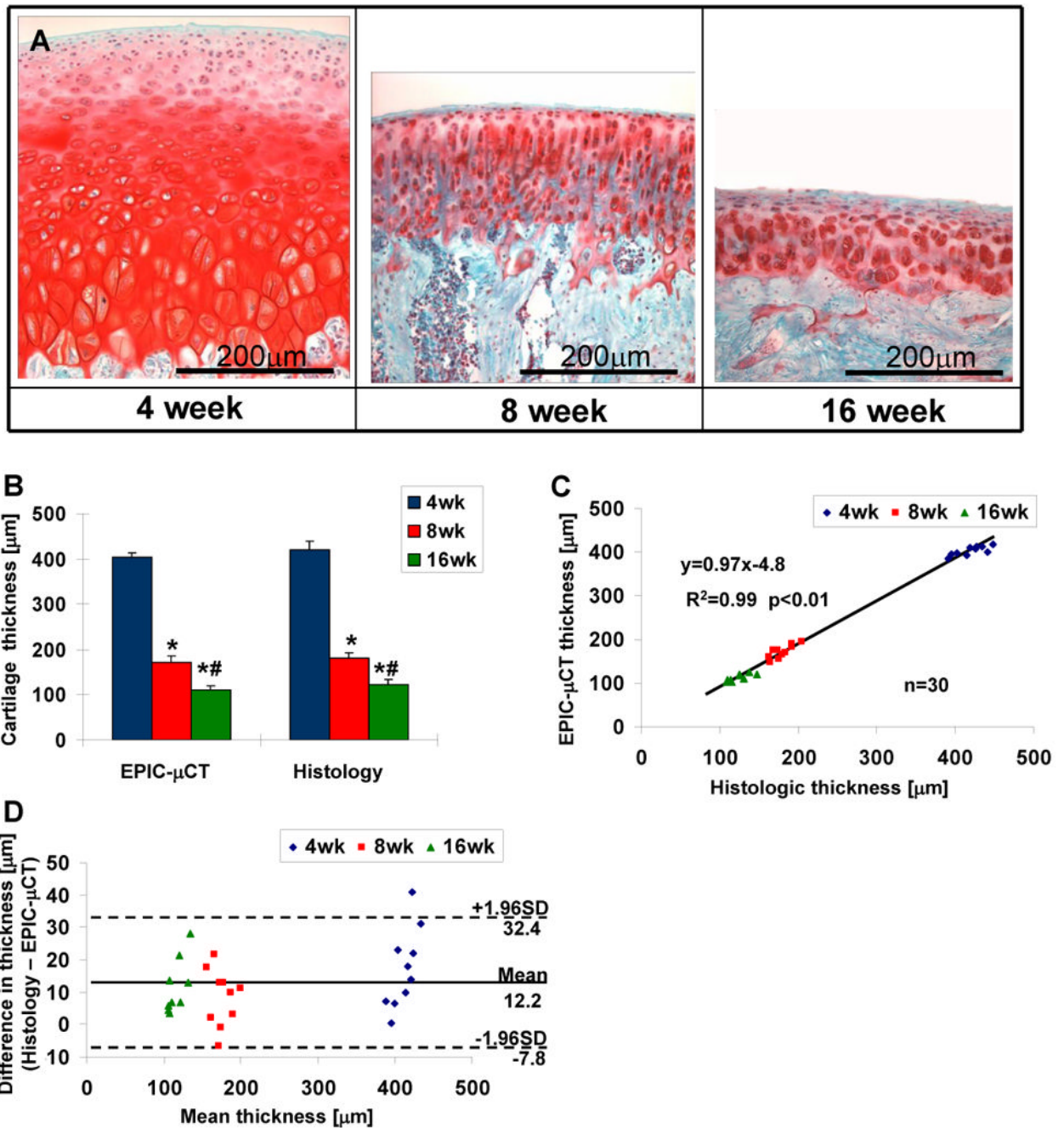
Figure 2.
Optimization of incubation time and Hexabrix concentration for EPIC-μCT in the rat model.
(A) The volume of analysis for each femoral condyle extended from the top surface of the
cartilage down 31 slices, or 372 μm, which included cartilage, subchondral bone, and some
trabecular bone. (B) The average attenuation of femoral articular cartilage after incubation with
each concentration of Hexabrix solution indicated that 30 min of incubation was sufficient for
Hexabrix to reach equilibration, regardless of the concentration. Representative X-ray
attenuation histograms for femoral articular cartilage and bone incubated in 20% (C), 30% (D),
40% (E) and 50% Hexabrix solution (F).

Figure 3.
Validation of EPIC-μCT thickness measurements for rat tibial articular cartilage via needle probe testing. (A) An illustration of needle probe testing on tibial articular cartilage. (B) Representative force versus displacement curve showed regions of changing slope that indicated contact with cartilage and bone surfaces. The inset displayed magnified data for the cartilage contact region. (C) Strong linear relationship between measurements of cartilage thickness obtained by EPIC-μCT and needle probing (slope=0.81, R^2=0.95, n=43). (D)The differences (needle probing - EPIC-μCT) versus average cartilage thickness measured by needle probing and EPIC-μCT with 95% limits of agreement.

Figure 4.
Evaluation of articular cartilage morphology during growth in male Wistar rats at 4, 8, and 16 weeks of age. (A) Representative images for intact distal femora, including bone (grey) and articular cartilage (white). (B) Representative thickness maps of segmented femoral articular cartilage. (C) Representative sagittal sections of each distal femur. Average cartilage volume (D), thickness (E), and surface area (F) for each age group (n=5, error bars indicate ± SD). * p<0.01 vs 4-week-old rats, # p<0.01 vs 8-week-old rats.

Figure 5.
Histologic evaluation of rat femoral articular cartilage from male Wistar rats at 4, 8, and 16 weeks of age for validation of EPIC-μCT measurements. (A) Representative images from safranin-O staining of femoral articular cartilage. (B) Average thickness of femoral articular cartilage assessed via EPIC-μCT and histology (n=10, error bars indicate ± SD). (C) Strong linear relationship between measurements of cartilage thickness obtained by EPIC-μCT and histology (slope = 0.97, $R^2 = 0.99$). (D) The differences (histology - EPIC-μCT) versus average cartilage thickness measured by histology and EPIC-μCT with 95% limits of agreement (n=30). * $p<0.01$ vs 4-week-old rats, # $p<0.01$ vs 8-week-old rats.